Catalysis Today 137 (2008) 418–422

Contents lists available at ScienceDirect

Catalysis Today

journal homepage: www.elsevier.com/locate/cattod

Decomposition of N_2O over the surface of cobalt spinel: A DFT account of reactivity experiments

Witold Piskorz [a], Filip Zasada [a], Paweł Stelmachowski [a], Andrzej Kotarba [a], Zbigniew Sojka [a,b,*]

[a] Faculty of Chemistry, Jagiellonian University, ul. Ingardena 3, 30-060 Kraków, Poland
[b] Regional Laboratory for Physico-Chemical Analyses and Structural Research, Jagiellonian University, Ingardena 3, 30-060 Kraków, Poland

ARTICLE INFO

Article history:
Available online 1 May 2008

Keywords:
DFT
Co_3O_4
Spinel
Cobalt
N_2O
Mechanism
Molecular modeling
Decomposition
deN_2O
Inhibition

ABSTRACT

The DFT molecular modeling of N_2O decomposition over cobalt spinel (1 0 0) plane was performed using a cluster approach, and applied to rationalize the experimental reactivity data. The energetics of the postulated elementary steps such as N_2O adsorption, N_2O activation through dissociative electron or oxygen atom transfer, surface diffusion of resultant oxygen intermediates, and their recombination into O_2, was evaluated and discussed. The geometry and electronic structure of the implicated active sites and intermediates were determined. Three different transition states were found for the activation of nitrous oxide molecule. In the preferred electron transfer mechanism, involving a monodentate transition state, the N_2O activation and the formation of dioxygen are energetically the most demanding steps, whereas the barrier for the oxygen surface diffusion was found to be distinctly smaller. For the oxygen atom transfer the reaction is energetically constraint by the N–O bond-breaking step. The inhibiting effect of co-adsorbed water and oxygen on the particular reaction steps was briefly addressed.

© 2008 Elsevier B.V. All rights reserved.

1. Introduction

The AB_2O_4 oxides of spinel structure containing 3d transition metal ions have a long record of wide scientific interest, owing to their remarkable electronic, magnetic, and catalytic properties [1–4]. In the latter context, the cobalt spinel $Co^{II}Co^{III}{}_2O_4$, and its derivates obtained by partial substitution with 2p, 3d and 4f dopants have recently received considerable attention as promising catalytic materials for direct decomposition of nitrous oxide into nitrogen and oxygen [5,6]. Being thermodynamically quite stable, highly divided spinels are also formed from mixed oxides produced by decomposition of hydrotalcites, and exhibit high activity in the deN_2O process [7]. Quite recently, excellent reactivity of doped cobalt spinels obtained by a simple precipitation method has been reported [8,9]. The catalytic activity of spinels depends essentially on the degree of substitution and the occupation of the tetrahedral and octahedral sites. The preparation method of the spinel precursors determines final oxide texture, surface composition and plays a crucial role in ultimate performance of these materials [8]. Some of them have been found to be active and stable enough for potential industrial applications for the low-temperature N_2O removal in nitric acid plants. However, the co-reactants present in the tail gases can be easily accumulated on the surface of the catalyst at such conditions and severely inhibit the deN_2O activity.

The kinetic of N_2O decomposition over oxide materials containing transition metal ions has been extensively investigated to find the correlation between the electronic structure of the catalysts (characterized essentially by their electron donor properties) and their reactivity [10–12]. Several mechanisms of N_2O decomposition, in the absence and presence of inhibitory gases (O_2, H_2O), based on experimental investigations [4,6,7,13] and theoretical modeling [14,15] have been proposed. In its simplest form, the putative mechanistic steps usually involve the interaction of a gas phase N_2O with the active sites, followed by its decomposition giving rise to a N_2 molecule and surface oxygen. The latter can be eliminated either by recombining with another oxygen atom (Langmuir–Hinshelwood mechanism) or by direct reaction with the intact N_2O molecule (Eley–Rideal mechanism). Since essentially these mechanistic considerations have been based on kinetic studies performed on various catalytic systems, an in-depth understanding of the molecular nature of the involved reaction active sites and intermediates is rather limited. Despite the extensive experimental studies on the deN_2O reaction over spinels, corroborative molecular modeling is still lacking.

* Corresponding author at: Faculty of Chemistry, Jagiellonian University, ul. Ingardena 3, 30-060 Kraków, Poland. Tel.: +48 12 663 20 17; fax: +48 12 634 05 15.
E-mail address: sojka@chemia.uj.edu.pl (Z. Sojka).

0920-5861/$ – see front matter © 2008 Elsevier B.V. All rights reserved.
doi:10.1016/j.cattod.2008.02.027

The aim of this work is to provide a primary theoretical account of the principal reaction steps including the obstructive effect of oxygen and water on the performance of the Co_3O_4 catalyst. To our knowledge it is the first mechanistic DFT insight into the deN_2O decomposition over cobalt spinel system.

2. Computational and experimental details

For all embedded cluster computations the DFT level of theory was chosen with RPBE [16] correlation-exchange (xc) potential (GGA) and DZP-quality numerical basis set with DSPP relativistic pseudopotential [17] for the core electrons, as implemented in DMol3 code [18,19]. The optimization of the geometry followed the BFGS scheme [20], whereas the transition state (TS) was determined by the use of the LST/QST scheme [21]. Computational models were built using the coordinates taken from the database spinel structure included in the Cerius2 package [22], and then both fractional coordinates and the unit cell dimensions were fully re-optimized in solid-state calculations using the CASTEP program [23]. The reaction pathways were computed within the embedded cluster scheme. The $Co_{18}O_{24}$ cluster was embedded in the 2156 point charge (PC) lattice. Both the positions of the PCs and their values (obtained from Hirshfeld population analysis [24]) were taken from an optimized solid-state structure. Both the stoichiometry and the electroneutrality of the cluster and the PC array were preserved.

The Co_3O_4 spinel samples were prepared by the precipitation method by the gradual addition of 15 wt.% aqueous solution of K_2CO_3 (POCh) to 19 g of $Co(NO_3)_2$ (Aldrich) diluted in 30 ml of distilled water at room temperature until the pH of the solution reached 9. The resultant precipitate was washed until the pH of filtrate was 7, and dried at 100 °C overnight, followed by calcination at 400 °C in air for 2 h. The samples were characterized by XRD, N_2-BET, and their reactivity in N_2O decomposition, in the absence and presence of water and oxygen, was evaluated in TPSR experiments. The phase verification of the materials was performed by the X-ray diffraction using an X'pert Pro Philips powder diffractometer with the Cu Kα radiation in a Bragg–Brentano geometry. The BET measurements were carried out by means of a Quntasorb Junior Instrument.

The temperature-programmed surface reaction measurements were performed in a quartz flow reactor using 500 mg of the catalyst in the form of sieve fraction of 0.2–0.3 mm. The reactant (5% N_2O/He, (5% N_2O + 1% H_2O)/He and (0.15% N_2O + 3% O_2)/He) flow rate of 7000 h^{-1}, and the heating rate of 10 °C/min in the range of 20–700 °C were used. The gas phase composition was monitored by a mass spectrometer (SRS RGA200, Stanford Research System).

3. Results and discussion

The results of the Co_3O_4 catalytic reactivity in the N_2O decomposition expressed as the Celsius temperature of 50% conversion ($T_{50\%}$) for various feed compositions of N_2O, O_2, and H_2O are shown in the form of the box plot in Fig. 1. Together with our experimental data we have added some recent literature values measured in similar conditions [8,9]. The well-known harmful effect of oxygen, water as well as water and oxygen jointly on the conversion, observed in the temperature range of 300–400 °C, can be clearly recognized. The influence of both inhibitors is quite similar (shifting up the average value of $T_{50\%}$ by about 30 °C). The activity is further suppressed (by additional 30 °C), when both inhibitors are present simultaneously. These phenomena are thus extremely important for the potential applications of cobalt spinel in the most challenging but economically appealing low-temperature regime, as a promising generic catalytic material for N_2O removal from the tail gases of nitric acid plants. Similar behavior

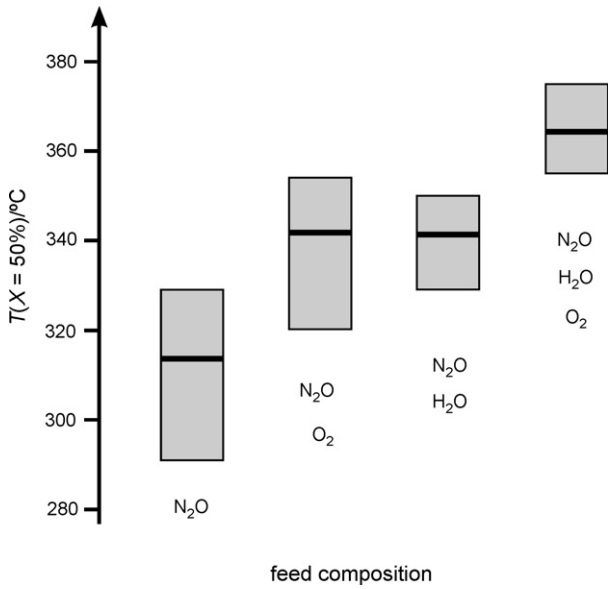

Fig. 1. The experimental results (including literature data [8,9]) of the temperature-programmed catalytic N_2O decomposition (expressed as the Celsius temperature of 50% conversion) over the cobalt spinel catalysts for different feed composition (0.1–5% N_2O, 0.1–5% N_2O + 1–5% H_2O, 0.1–0.15% N_2O + 3–10% O_2, 0.1–0.15% N_2O + 3–10% O_2 + 1–5% H_2O in helium) and a space velocity (GHSV) in the range 5000–15 000 h^{-1}. The grey boxes show the observed temperature ranges of the 50% of N_2O conversion, whereas the black bars correspond to their weighted averages.

was already observed for many other oxide systems [3,8,9], but until now none of them have ever been developed into the stage of practical application. One of the reasons for such a situation may be related to the fact that judicious optimization of the catalyst is difficult to achieve without a more in-depth understanding of the reaction mechanism at the molecular level.

The cobalt spinel structure is constituted by cubic closed pack arrangement of O^{-2} anions with the trivalent octahedral cobalt ions in the low spin state ($t_{2g}^6 e_g^0$) $S = 0$, and the tetrahedral Co^{2+} with the high spin configuration ($e^4 t_2^3$), $S = 3/2$. Since the tetrahedral sites are rather well separated, the magnetic interaction between them is weak [1], and the divalent cobalt ions behave as isolated paramagnetic sites. As a result the structure is rather easily amenable for DFT modeling. The substitution experiments in the spinel structure suggest that the octahedral cobalt ions are active in N_2O decomposition [6,8].

The structure of the $Co_{18}O_{24}$ PC_{2156} cluster used for the DFT calculations is shown in Fig. 2a. However, for the sake of simplicity in the artwork, hereafter this cluster will be represented by a smaller epitome shown in Fig. 2b. The characteristic feature of the modeled (1 0 0) termination of the spinel surface is its corrugation with the exposed octahedral and recessed tetrahedral cobalt ions. The calculated oxygen–cobalt distances are in the range 1.938–1.993 Å and compare well with the experimental values of 1.946 and 1.948 Å for tetrahedral and octahedral coordination, respectively. The calculated angles $\angle(O\text{–}Co^T\text{–}O) = 109.47°$ for tetrahedral Co are in remarkable agreement with the experimental value of 109.47° and indicate that the tetrahedral sites are essentially not distorted. For the octahedral sites two types of $\angle(O_{ax}\text{–}Co^O\text{–}O_{eq})$ angles, equal to 96.58° and 83.41°, were found, whereas the angle $\angle(O_{ax}\text{–}Co^O\text{–}O_{ax})$ equals to 177.69°. All of them are very close to the corresponding crystallographic values of 96.11°, 83.89° and 180°, respectively, implying a D_{3d} local site symmetry of the octahedral cobalt ions.

From the analysis of the available mechanistic schemes inferred from previous kinetic studies [6,7], the following reaction steps

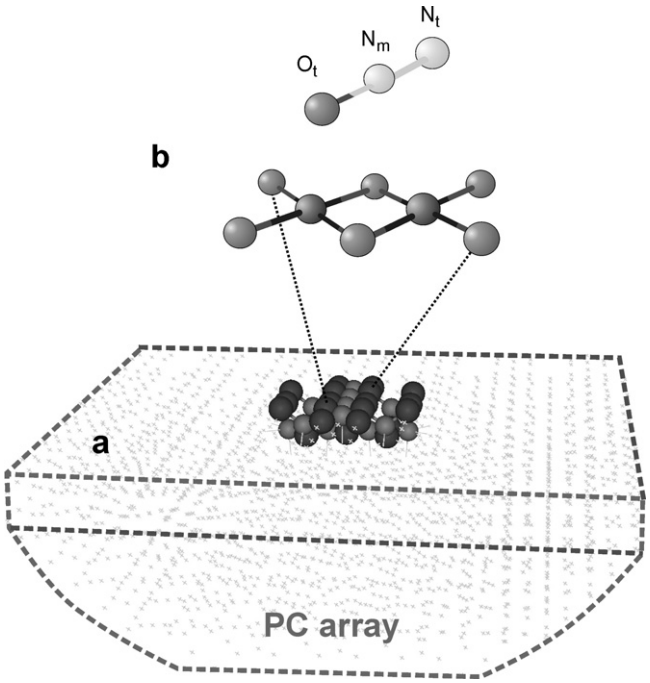

Fig. 2. Embedded cluster model ($Co_{18}O_{24}$ PC_{2156}) of the (1 0 0) surface of the cobalt spinel used in DFT computations (a), and its epitome used in the artwork of this paper, for the sake of simplicity (b).

were considered in the DFT modeling: activation of N_2O on cobalt and oxygen surface sites (Fig. 3a–e), oxygen surface diffusion (Fig. 3f–h) and recombination of the peroxy intermediates to form O_2 molecule followed by its desorption (Fig. 3i–j). The proposed pathway is one of several possible scenarios, especially if defects and heterogeneity are taken into account, and conceivably represents the simplest scheme taking place at a non-defected (1 0 0) surface. The monodentate η^1-O mode of N_2O adsorption on the Co site with the energy of ~3 kcal/mol and the distance Co–ON_2 of ~3 Å was found to be quite weak. The electronic structure of the adsorbed N_2O molecule remained essentially intact, since the N_m–N_t, and N_m–O_t bond lengths of 1.17 and 1.14 Å were virtually the same as in the gas molecule. Thus, this mode can be associated with physisorption, in-line with the experiment, where appreciable molecular N_2O adsorption was not observed at the reaction conditions, and therefore cannot be treated adequately by the DFT method. The metastable η^2-(O, N) mode of adsorption to two surface Co ions (shown in grey in Fig. 3b) is located at higher energy (5.6 kcal/mol), and is associated with more pronounced changes in the N_2O geometry. The Co–ON_2 distance is shorter (2.11 Å), whereas N_m–O_t bond length increases to 1.26 Å with the N_m–N_t bond remaining unchanged (1.17 Å). This adsorbed state, however, seems to be kinetically less accessible, as a more demanding dual-site event preceded by N_2O bending. As a result the Eley–Rideal is the most likely route of N_2O activation in accordance with the kinetic models [6,7].

The next step of the reaction involves N–O bond cleavage, which can follow one of three possible redox pathways [25]. The anionic one (η^1-O{O^{2-}}) consists formally in oxygen atom transfer from the gas phase N_2O molecule to the surface O^{2-}, leading to the formation of the peroxy (O_2^{-2}) intermediate (Fig. 3g). The transition state for this process (Fig. 3c) is located at 56.6 kcal/mol, implying that such a pathway is kinetically hindered. Overall, the process is slightly endoenergetic (by 3.2 kcal/mol), and the Hirshfeld population analysis shows that the partial charge ($q_O = -0.18$) in the resultant moiety (O_m–O_{surf}) is equally distributed, which indeed is tantamount with the formation of the surface peroxy group. However, as implied by Fig. 3, there are two other energetically more favorable pathways of surface peroxy group formation. They involve the cationic η^1-O{Co} (Fig. 3d) and η^2-(O, N){Co, Co} (Fig. 3e) transition states, for the gas phase and the adsorbed N_2O molecule, respectively, followed by the surface diffusion of oxygen intermediate (Fig. 3f–h).

The above-mentioned alternative pathways, initiated by the electron transfer from the surface cobalt sites to the empty $3\pi^*$ orbital of the N_2O molecule, lead formally to transient bent N_2O^- attached via monodentate η^1-O{Co} and bidentate η^2-(O, N){Co,

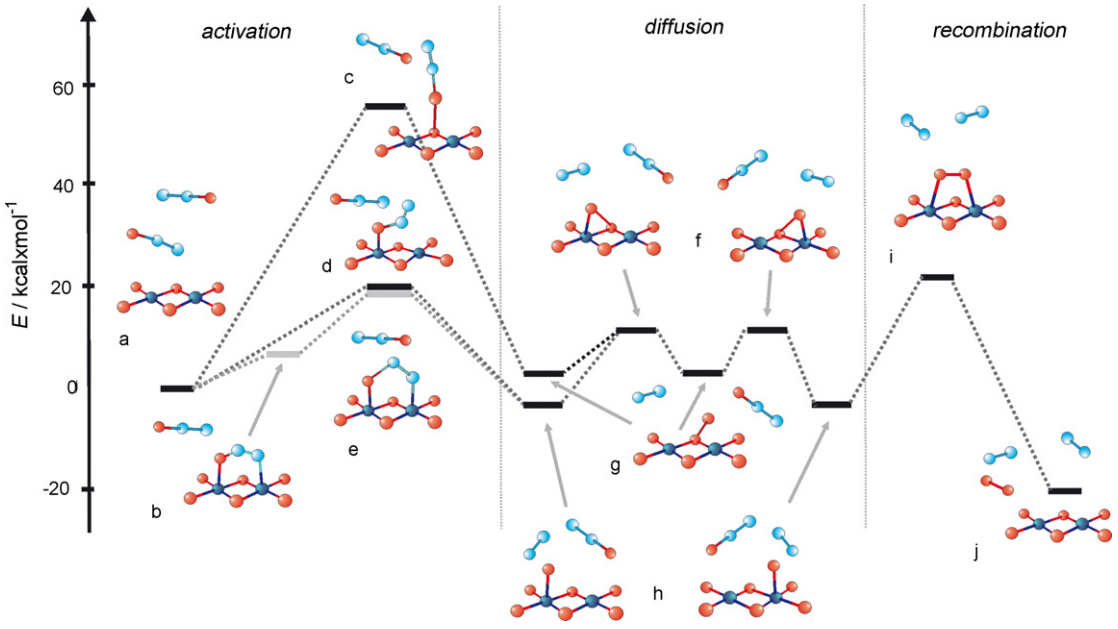

Fig. 3. Energetic profile of the principal steps of N_2O decomposition over (1 0 0) surface of Co_3O_4: activation of N_2O (a–e), surface diffusion of oxygen intermediates (f–h), recombination of oxygen followed by desorption of O_2 (i and j). The non-preferred activation pathway (b–e) is shown in grey. In the diagram the grey arrows assign the molecular structures to the corresponding energy levels.

Co} modes. They require only 20.1 and 19.6 kcal/mol to reach the corresponding transition state configurations (Fig. 3d and e). It is known from the experiments of electron attachment to nitrous oxide that owing to the particular electronic structure of N_2O and N_2O^-, the N–O bond is spontaneously cleaved with a low activation energy (E_A = 11 kcal/mol), once the LUMO orbital is populated [26]. Since the neutral N_2O molecule in the ground state is linear, whereas the corresponding N_2O^- transient is angular, the electron transfer is preceded by N_2O bending, following the Franck–Condon principle. Indeed, the geometry of both transition states reflects clearly this picture and is characterized by strong elongation of the N–O bond (1.61 and 1.38 Å for the mono and bidentate forms, respectively), and bending of the N_2O moiety with the corresponding $\angle(O_t–N_m–N_t)$ angles of 126.7° and 130.85°, respectively. Closer inspection of the monodentate TS (Fig. 3d) shows that the insipient Co–O bond equals to 1.91 Å. The partial charge on the cobalt site is enhanced from 0.27 to 0.35, whereas on oxygen it changes from −0.07 to −0.19. At the same time the charges on the middle ($q_{N_m} = +0.16$) and terminal ($q_{N_t} = -0.09$) nitrogen atoms become essentially neutralized ($q_{N_m} = +0.03, q_{N_t} = +0.01$). In the case of the bidentate TS (Fig. 3e) the partial charge of cobalt increases to +0.42, whereas on oxygen it decreases to −0.21, indicating again that the N_2O cationic activation occurs through significant transfer of the electron density. Similarly, the charges on the middle nitrogen and on the terminal nitrogen atoms are also substantially reduced to $q_{N_m} = +0.05$ and $q_{N_t} = -0.01$, respectively, indicating the formation of an incipient N_2 molecule. The Co–O bond of 1.78 Å was quite close to the equilibrium value of 1.72 Å observed in the resultant {Co–O} intermediate species (Fig. 3h). The Hirshfeld charge analysis of the η^1-O{Co} and η^2-(O, N){Co, Co} transition states revealed that N_2O activation has an oxidative character involving strong charge redistribution within the reactive units. Despite the distinct differences in the Co–O and O–N bond lengths changes, the common feature of both transition states is the strong polarization of the Co–O bond accompanied by concomitant ceasing of the polarity of the N–N moiety, characteristic of the covalent bond formation. The nascent N_2 molecule can be thus released to the gas phase quite readily in the next step. Despite the bidentate transition state is even slightly lower in energy than the monodentate one, it is accessible via a kinetically less unfavorable metastable adsorbed state, and therefore essentially the monodentate transition state (Fig. 3d) seems to provide the principal route for N_2O activation actually.

The next mechanistic step involves diffusion of the reaction intermediates formally regarded as O^- ions (Fig. 3f–h). The analysis of possible surface diffusion pathways indicated that the direct hopping of oxygen along the adjacent cobalt sites is rather unfavorable due to the large $d_{Co–Co}$ distance (2.98 Å). As a result, the surface migration takes place through the intermediary of surface O^{2-} ions. It is accompanied by the transfer of the electron density from the traveling oxygen atom back to the cobalt centers (q_{Co} changes from +0.42 to +0.27), restoring the active sites. The resultant oxygen atom is drawn toward the O^{2-} surface anion and by gaining the negative charge of −0.34 (at the expense of the lattice oxygen) turns into an O_2^{2-} intermediate. The corresponding transition state situated at 12.4 kcal/mol is shown in Fig. 3f together with the geometry of the peroxy species. Noting the distance between O^{2-} ions ($d_{O–O}$ = 2.56 Å) the migration of oxygen across the surface by hopping over the anionic sites is, for the same reason as in the case of the cobalt sites, energetically also unfavorable. As a result the diffusion occurs by passing from cationic to anionic sites consecutively, with rather low-energy barriers (12.4 and 6.5 kcal/mol, respectively). Thus, the oxygen atom migration exhibits a pronounced redox character as it is accompanied by concomitant alternation of the partial charges of the implicated cobalt and oxygen sites.

The diffusive recombination of the surface oxygen intermediates (Fig. 3i), which closes the catalytic cycle, appears to be energetically more demanding that the surface diffusion step. It starts by an encounter of two migrating oxygen intermediates on adjacent cobalt sites. They interact mutually forming a dioxygen precursor at the O–O distance of 1.38 Å. Both oxygen atoms still bear slightly negative charges ($q_{O_1} = q_{O_2} = -0.05$), distinctly different from that in the peroxy intermediate ($q_{O_1} = -0.18$, and $q_{O_2} = -0.16$). This means that the formation of the insipient O–O bonding is accompanied by the flow of the electron density from oxygen back to the cobalt sites. In the transition state located at 23.4 kcal/mol, the O–O distance decreases to 1.28 Å and the atomic charges to $q_{O_1} = q_{O_2} = -0.01$. The nascent O_2 molecule still retains the parent singlet state, resembling therefore a bound singlet oxygen ($^1\Delta_g$). The singlet to triplet crossing occurs at the energy of 4 kcal/mol below the transition state, with the O–O distance (1.20 Å) approaching the equilibrium bond length (1.11 Å) of the final dioxygen molecule ($^3\Sigma_g^-$) as shown in Fig. 3j.

The brief survey of the experimental results (Fig. 1) shows a distinct inhibiting effect of water and oxygen, typically present in the real feed, on catalytic performance of Co_3O_4. Although any detailed molecular elucidation of the inhibiting effects requires more thorough investigations, preliminary hints can be already inferred from DFT results of simple water and oxygen adsorption. Water adsorbed associatively on a cobalt center is additionally stabilized by two neighboring surface oxygen atoms, which leads to resultant adsorption energy of 14 kcal/mol and exhibits an electron donor character. The corresponding dissociative mode with 30 kcal/mol is apparently much more stable. Among two possible adsorption states of oxygen, top-on η^1 and side-on η^2, the latter was found to be stronger with the adsorption energy of 19 kcal/mol. These values show clearly that water and oxygen molecules exhibit higher energetic affinity toward the investigated Co_3O_4 (1 0 0) surface than the N_2O reactant and its descent intermediates, and provide the support for the inhibiting effect observed when both molecules are present in the feed. Besides the blocking of active sites co-reactants may also influence redox properties of the spinel surface revealed by the work function changes upon adsorption [27]. The latter effect shall influence particularly those steps where the changes in the partial charge are the most important, i.e., the activation and diffusion steps. Whereas, for the oxygen recombination (Fig. 3i), which is accompanied by relatively small charge redistribution, the influence of co-adsorbents is expected to be of less significance.

4. Conclusions

DFT molecular modeling was used for investigations of the principal mechanistic steps of N_2O decomposition over the cobalt spinel (1 0 0) surface. The reaction route was discussed in terms of the energy, geometry, and partial charges of the involved active sites, reactants and intermediates. It was found that in the preferred electron transfer mechanism, involving a monodentate transition state, the N_2O activation (E_a = 20.1 kcal/mol) and recombination of surface oxygen atoms (E_a = 23.4 kcal/mol) are energetically the most demanding steps. Whereas for the oxygen-transfer route the reaction is essentially constrained by the high activation energy of the N–O bond breaking (E_a = 56.6 kcal/mol). Surface diffusion of oxygen intermediates, occurs by successive hopping between cationic and anionic sites with energy barriers of 12.4 and 6.5 kcal/mol, respectively. It is accompanied by concomitant alternation of the partial charges of the implicated cobalt and oxygen sites. The observed poisoning by water and oxygen was associated mainly with site blocking effect of the co-adsorbed species.

Acknowledgements

This work has been supported by Polish Ministry of Science and High Education within the project Eureka STATIONOCAT E! 3230. We would like to thank Mike Green for linguistically editing this manuscript.

References

[1] J.B. Goodenough, Magnetism and Chemical Bond, Interscience, New York, 1963.
[2] V.E. Henrich, P.A. Cox, The Surface Science of Metal Oxides, Cambridge University Press, Cambridge, 1994.
[3] A.A. Vargas-Tah, R.C. García, L.F.P. Archila, J.R. Solis, A.J.G. López, Catal. Today 107 (2005) 713.
[4] N. Russo, D. Fino, G. Saracco, V. Specchia, Catal. Today 119 (2007) 228.
[5] L. Yan, T. Ren, X. Wang, Q. Gao, D. Ji, J. Suo, Catal. Commun. 4 (2003) 505.
[6] F. Kapteijn, J. Rodriguez-Mirasol, J.A. Moulijn, Appl. Catal. B: Environ. 9 (1996) 25.
[7] L. Obalova, V. Fila, Appl. Catal. B: Environ. 70 (2007) 353.
[8] L. Yan, T. Ren, X. Wang, Q. Gao, D. Ji, J. Suo, Appl. Catal. B: Environ. 45 (2003) 85.
[9] C. Ohanishi, K. Asano, S. Iwamoto, K. Chikama, M. Inoue, Catal. Today 120 (2007) 145.
[10] A. Scagnelli, C. Di Valentin, G. Pacchioni, Surf. Sci. 600 (2006) 386.
[11] R.S. Drago, K. Jurczyk, N. Kob, Appl. Catal. B: Environ. 13 (1997) 69.
[12] A.L. Yakovlev, G.M. Zhidomirov, R.A. van Santen, Catal. Lett. 75 (2001) 45.
[13] L. Obalova, K. Jiratova, F. Kovanda, M. Valaskova, J. Balabanova, K. Pacultova, J. Mol. Catal. A 248 (2006) 210.
[14] X. Lu, X. Xu, N. Wang, Q. Zhang, J. Phys. Chem. B 103 (1999) 3373.
[15] A. Spis, H. Miettinen, J. Phys. Chem. B 102 (1998) 2555.
[16] B. Hammer, L.B. Hansen, J.K. Norskov, Phys. Rev. B 59 (1999) 7413.
[17] B. Delley, Phys. Rev. B 66 (2002) 155125.
[18] B. Delley, J. Chem. Phys. 92 (1990) 508.
[19] http://www.accelrys.com/products/mstudio/modeling/quantumandcatalysis/dmol3.html
[20] T.H. Fischer, J. Almlof, J. Phys. Chem. 96 (1992) 9768.
[21] T.A. Halgren, W.N. Lipscomb, Chem. Phys. Lett. 49 (1977) 225.
[22] http://www.accelrys.com/products/cerius2/
[23] http://www.tcm.phy.cam.ac.uk/castep/
[24] F.L. Hirshfeld, Theor. Chim. Acta B 44 (1977) 129.
[25] P. Pietrzyk, F. Zasada, W. Piskorz, A. Kotarba, Z. Sojka, Catal. Today 119 (2007) 219.
[26] Z. Sojka, Appl. Magn. Reson. 18 (2000), 71 and the references therein.
[27] P. Stelmachowski, A. Adamski, A. Kotarba, Z. Sojka, Proc of the XXXIX Annual Polish Conference on Catalysis, Krakow, (2007), p. 347.